



## Patterns of interannual climate variability in large marine ecosystems



Helena Cachanhuk Soares <sup>a,\*</sup>, Douglas Francisco Marcolino Gherardi <sup>a</sup>, Luciano Ponzi Pezzi <sup>a</sup>, Mary Toshie Kayano <sup>b</sup>, Eduardo Tavares Paes <sup>c</sup>

<sup>a</sup> Divisão de Sensoriamento Remoto – Instituto Nacional de Pesquisas Espaciais (INPE), Av. dos Astronautas, 1758, São José dos Campos, SP 12227-010, Brazil

<sup>b</sup> Centro de Previsão de Tempo e Estudos Climáticos (CPTEC) – INPE, Rodovia Presidente Dutra, km 39, Cachoeira Paulista, SP 12630-000, Brazil

<sup>c</sup> Instituto Socioambiental e dos Recursos Hídricos (ISARH), Universidade Federal Rural da Amazônia, Avenida Presidente Tancredo Neves 2501, Belém, PA 66077-901, Brazil

### ARTICLE INFO

#### Article history:

Received 30 September 2013

Received in revised form 28 February 2014

Accepted 3 March 2014

Available online 12 March 2014

#### Keywords:

Large marine ecosystems  
Ocean–atmosphere system  
South Atlantic climate variability  
Climatic changes  
Ecosystem management  
Correlation analysis

### ABSTRACT

The purpose of this study is to investigate the vulnerability of the Brazilian and western African Large Marine Ecosystems (LMEs) to local and remote forcing, including the Pacific Decadal Oscillation (PDO) regime shift. The analyses are based on the total and partial correlation between climate indices (Niño3, tropical South Atlantic (TSA), tropical North Atlantic (TNA) and Antarctic oscillation (AAO) and oceanic and atmospheric variables (sea surface temperature (SST), wind stress, Ekman transport, sea level pressure and outgoing longwave radiation). Differences in the correlation fields between the cold and warm PDO indicate that this mode exerts a significant impact on the thermodynamic balance of the ocean–atmosphere system on the South Atlantic ocean, mainly in the South Brazil and Benguela LMEs. The PDO regime shift also resulted in an increase in the spatial variability of SST and wind stress anomalies, mainly along the western African LMEs. Another important finding is the strong AAO influence on the SST anomalies (SSTA) in the South Brazil LME. It is also striking that TSA modulates the relation between El Niño–Southern Oscillation (ENSO) and SSTA, by reducing the influence of ENSO on SSTA during the warm PDO period in the North and East Brazil LMEs and in the Guinea Current LME. The relation between AAO and SSTA on the tropical area is also influenced by the TSA. The results shown here give a clear indication that future ecosystem-based management actions aimed at the conservation of marine resources under climate change need to consider the high complexity of basin-scale interactions between local and remote climate forcings, including their effects on the ocean–atmosphere system of the South Atlantic ocean.

© 2014 Elsevier B.V. All rights reserved.

### 1. Introduction

Warming trends reported for the world's Large Marine Ecosystems (LMEs) have been associated with contrasting impacts on zooplankton and fisheries biomass, even for close geographic locations within an ocean basin (Sherman et al., 2009). The inferred warming rate (measured as a linear trend) is not the same everywhere, instead, it may vary from slow (over 0.05 °C/decade) to super-fast (over 0.45 °C/decade) (Belkin, 2009). The effects of these warming trends are not uniform, the fast-warming scenario for the northern Northeast Atlantic LMEs resulted in an increase in fisheries biomass due to increased zooplankton biomass while southern areas of these LMEs experienced fisheries biomass declines (Sherman et al., 2009). The response of fisheries biomass to remote and local climate forcing tend to be diverse as a result of amplifications, time lags and feedbacks inducing abrupt and discontinuous shifts (Overland et al., 2010), leading to contrasting biomass yields (Soares et al., 2011). So, before the actual influence of environmental trends

(e.g., increase in sea surface temperature) on the functioning of LMEs can be accurately quantified, the relative influence of local and remote forcings on environmental conditions needs to be assessed.

The sensitivity of the South Atlantic to climate variability at interannual, decadal and multidecadal timescales is closely related to changes in basin-scale sea surface temperature (SST) and sea level pressure (SLP) (Wainer and Venegas, 2002). The most important examples of the interplay between local and remote forcing of the SST variability in the tropical Atlantic are the coupled local ocean–atmospheric interaction and the El Niño–Southern Oscillation (ENSO), respectively (Nobre and Shukla, 1996; Wu et al., 2007). Kayano et al. (2012) showed that there is a SST mode in the South Atlantic, which they called the southwest South Atlantic mode. This is characterized by a dipolar structure with a strong negative center at (30°S, 40°W) that extends between 15°S and 45°S, and a less extensive positive center in the southern mid-latitudes, which is strongly modulated by the ENSO. They showed that an El Niño (La Niña) event precedes by up to 12 months the sea surface warming (cooling) in the South Atlantic between 15°S and 45°S. They also found that the South Atlantic SST dipole mode with centers at (15°S, 0° longitude) and (37.5°S, 25°W) leads or lags ENSO depending on the period of analysis.

\* Corresponding author. Tel.: +55 12 3186 8505; fax: +55 12 3101 2835.  
E-mail address: [helenacs@dsr.inpe.br](mailto:helenacs@dsr.inpe.br) (H.C. Soares).

Clearly, the response of the tropical Atlantic to remote forcing depends on atmospheric teleconnection mechanisms and on basin-scale SST gradients acting on different time scales (Alexander et al., 2002; Enfield and Mayer, 1997; Giannini et al., 2004; Hastenrath, 2006; Lanzante, 1996). Mechanisms include the upper-tropospheric Rossby-wave train that extends from the equatorial eastern Pacific to the northern tropical Atlantic and the east-west displacement of the Walker circulation during El Niño years (Hastenrath, 1976; Kayano et al., 1988). Alternatively, Chiang and Lintner (2005) suggested that the anomalous warming signal produced in the eastern tropical Pacific during an El Niño episode propagates eastwards in the troposphere as an equatorial Kelvin wave. This tropospheric warming originated from the ocean surface acts to reduce moist convection, causing the latent heat to accumulate at the boundary layer. So, as a result of the reduced evaporation the heat content builds up and warms the ocean mixed layer. In any case, there is still an acute lack of research on the response of the South Atlantic to remote and local forcing of the interannual time scale and their possible effects on the functioning of LMEs.

There are a number of forcing factors affecting the oceanic and atmospheric conditions along the South Atlantic LMEs. An important local forcing in the tropical Atlantic is the inter-hemispheric SST gradient (Andreoli and Kayano, 2003; Enfield and Mayer, 1997; Enfield et al., 1999; Giannini et al., 2004; Moura and Shukla, 1981; Nobre and Shukla, 1996; Pezzi and Cavalcanti, 2001; Servain et al., 2000; Wang, 2002). Simulations with a coupled ocean and atmosphere numerical model (Xie, 1999) indicate that the interactions between wind, SST and evaporation determine the growth and oscillation of the SST inter-hemispheric gradient (see also Chang et al., 2006). Enfield et al. (1999) summarized the temporal variability of the meridional SSTAs in the Atlantic using two climate indices that represent local modes: the Tropical South Atlantic (TSA) and the Tropical North Atlantic (TNA).

Another Atlantic local mode is the Antarctic Oscillation (AAO), also known as the Southern Hemisphere Annular Mode, and it represents the differences in surface pressure between middle and high south latitudes (Gong and Wang, 1999; Hall and Visbeck, 2002; Thompson and Wallace, 2000). Hall and Visbeck (2002) showed that this mode is associated with changes in the surface westerlies as a result of the poleward movement and intensification (weakening) of the atmospheric jet stream around 55°S (35°S). The oceanic linkage is through frictional transfer of momentum, causing Ekman flow anomalies as high as two-thirds of the mean value. It has been suggested (L'Heureux and Thompson, 2005) that the ENSO affects the AAO through changes in the zonal wind anomalies in the subtropical latitudes, accounting for 25% of AAO variability during austral summer.

Besides ENSO, another important remote forcing acting on the Atlantic basin is the Pacific Decadal Oscillation (PDO) (Mantua et al., 1997; Zhang et al., 1997). The PDO is best understood as the leading mode of interdecadal variability in SST of the extratropical North Pacific with characteristic cold and warm phases (MacDonald and Case, 2005). These cold and warm phases are known to trigger significant climate and biological regime shifts with impacts on important fish stocks (Chavez et al., 2003; Mantua and Hare, 2002). It has been shown that the amplitude and dominant period of ENSO in the Pacific have increased after 1976, concurrent with the Pacific shift driven by decadal changes in the background equatorial winds and associated upwelling (Wang and An, 2002). Although the PDO-induced regime shift is well documented for the biota of the North Pacific with a significant change between 1976 and 1977 (see Mantua and Hare, 2002), there is no information available so far as to how the cold and warm phases of the PDO could impact the physical environments along the South Atlantic LMEs. It is also unclear how PDO and ENSO would interact in a basin scale to generate spatial patterns of variations in SST, wind stress and Ekman transport that could be biologically relevant.

Here, we demonstrate for the first time the effects of local and remote forcing on the oceanic and atmospheric conditions along the Brazilian and western African coast LMEs, including the PDO regime

shift. We highlight that the geographical boundaries of these LMEs are largely offset from the spatial patterns of climate-induced variations that emerge from our analyses. Therefore, productivity and trophic relations in each of the LMEs are likely to generate mixed responses at the ecosystem level. If not taken into consideration by the environmental-based management policies, this has the potential to induce policy makers to react to a confounded scenario of environmental change. Maps of total and partial linear correlations between climate indices and oceanic-atmospheric variables in the South Atlantic are used to assess the vulnerability of the LMEs in this oceanic sector (Fig. 1) to climate variability.

## 2. Data and methodology

The SST data used here were the monthly gridded series for the period from 1948 to 2008, with a spatial resolution of 2° in latitude and longitude, derived from the version 3 of the reconstructed SST dataset, described by Smith et al. (2008). These data can be downloaded from <http://migre.me/3Hy49>. Wind stress data were obtained from the Simple Ocean Data Assimilation (SODA), which are in a spatial resolution of 0.5° in latitude and longitude and the period used in the analyses ranges from 1958 to 2001. The wind stress information was used to derive the Ekman transport ( $\vec{E}$ ,  $\text{kg m}^{-1} \text{s}^{-1}$ ) using the follow equation:

$$\vec{E} = \frac{\vec{k} \times \vec{\tau}}{f} \quad (1)$$

where  $\vec{k}$  is a unit vector directed vertically upward,  $\vec{\tau}$  ( $\text{kg m}^{-1} \text{s}^{-2}$ ) is the wind stress vector and  $f$  is the Coriolis parameter ( $\text{s}^{-1}$ ).

The outgoing longwave radiation (OLR) data employed in this work were derived from the polar-orbiting National Oceanic and Atmospheric Administration (NOAA) satellites that have a spatial resolution of 2.5° latitude-longitude over the period from 1979 to 2008. OLR can be used to distinguish deep convection processes and to estimate the radiation balance of the Earth (Liebmann and Smith, 1996). These data were downloaded from: [http://www.esrl.noaa.gov/psd/data/gridded/data.interp\\_OLR.html](http://www.esrl.noaa.gov/psd/data/gridded/data.interp_OLR.html). The SLP data used have a spatial resolution of 2.5° and were obtained from the National Centers for Environmental Prediction/National Center for Atmospheric Research (NCEP/NCAR) Reanalysis Project version 1 (Kalnay et al., 1996) for the period from 1948 to 2008. Monthly anomalies of the variables were computed at each grid point as the departures from the climatologies based on the period with available data (Table 1). Hereinafter, the anomalies of SST, SLP,

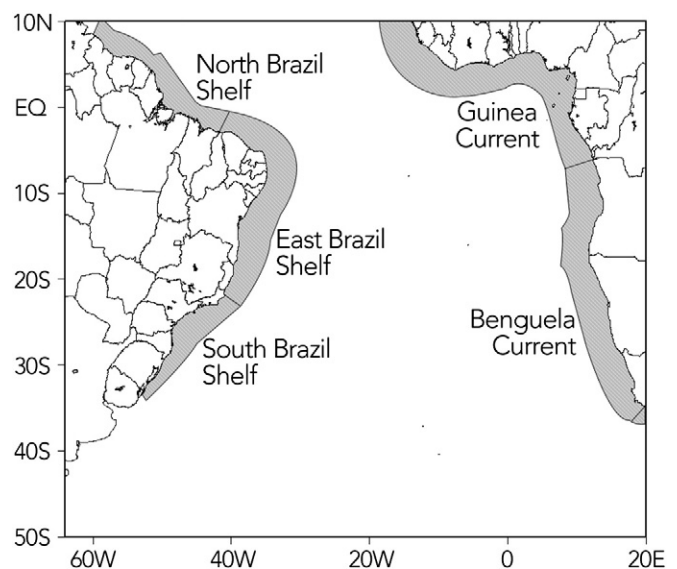


Fig. 1. Location of the South Atlantic LMEs in the region of interest.

**Table 1**

Description of variables: source, spatial resolution, period used to calculate the anomalies and the correlations and the PDO phases considered.

Variable	Source	Spatial resolution	Period	PDO phase analyzed
SST	ERSST v3 Smith et al. (2008)	$2 \times 2^\circ$	1948–2008	Cold and warm
Wind stress	SODA Carton and Giese (2008)	$0.5 \times 0.5^\circ$	1958–2001	Cold and warm
OLR	NOAA satellites Liebmann and Smith (1996)	$2 \times 2^\circ$	1979–2008	Warm
SLP	NCEP/NCAR Reanalysis 1 Kalnay et al. (2006)	$2.5 \times 2.5^\circ$	1948–2008	Cold and warm

OLR, wind stress and Ekman transport are referred to as SSTA, SLPA, OLRA, WSA and ETA respectively.

The climate indices used were: Niño3, Tropical North Atlantic (TNA), Tropical South Atlantic (TSA), and Antarctic Oscillation Index (AAO). The Niño3, TNA and TSA are based on the average SSTA for the areas bounded at  $5^\circ\text{S}$ ,  $5^\circ\text{N}$  and  $150^\circ\text{W}$ ,  $90^\circ\text{W}$  for Niño3; at  $5.5^\circ\text{N}$ ,  $23.5^\circ\text{N}$  and  $15^\circ\text{W}$ ,  $57.5^\circ\text{W}$  for TNA; and at  $0^\circ$ ,  $20^\circ\text{S}$  and  $10^\circ\text{E}$   $30^\circ\text{W}$  for TSA (Enfield et al., 1999; Kayano et al., 2009). The AAO (Kidson, 1988; Thompson and Wallace, 2000) is calculated by projecting the monthly mean 700 hPa geopotential height (normalized) anomalies poleward of  $20^\circ\text{S}$  onto the leading Empirical Orthogonal Function (EOF) mode of these anomalies from 1979 to 2000. This index has been used to describe the mass seesaw between the southern mid and high latitudes, with positive (negative) values representing above (below) normal geopotential height in the midlatitudes and below (above) normal geopotential height in the high latitudes. The AAO series was obtained from the Climate Prediction Center/National Oceanic and Atmospheric Administration (CPC/NOAA) at [http://www.cpc.noaa.gov/products/precip/CWlink/daily\\_ao\\_index/ao/ao\\_index.html](http://www.cpc.noaa.gov/products/precip/CWlink/daily_ao_index/ao/ao_index.html).

The SSTAs were linearly detrended and all the variables and indices were submitted to a band-pass filtering process based on the Morlet wavelet to retain only the interannual variability between 2 and 7 years (see Kayano et al., 2009 for details). For the filtering procedure we have used the Matlab (Mathworks) code described by Torrence and Compo (1998). The terms ENSO and Niño3 refer, respectively, to the climatic phenomenon and the index used as its proxy.

Maps of total correlation between the indices and ocean-atmospheric variables were calculated for the monthly data series to assess their linear relations,

$$\rho_{x,y} = \frac{\sum_{i=1}^n (x_i - \bar{x})(y_i - \bar{y})}{\sqrt{\sum_{i=1}^n (x_i - \bar{x})^2} \sqrt{\sum_{i=1}^n (y_i - \bar{y})^2}} \quad (2)$$

where,  $x$  and  $y$  are the correlated variables with  $n$  elements,  $\bar{x}$  and  $\bar{y}$  are the average values of these variables.

The relative effects of local indices (TSA and TNA) on the remote forcing (ENSO) were examined. Also, the effects of the TSA, TNA and ENSO on a given variable while the AAO effect is excluded were also analyzed. These analyses were based on the partial correlation coefficients calculated from:

$$\rho_{12,3} = \frac{\rho_{12} - \rho_{13} \cdot \rho_{23}}{\sqrt{1 - \rho_{13}^2} \sqrt{1 - \rho_{23}^2}} \quad (3)$$

where  $\rho_{12,3}$  is the partial correlation between variables 1 and 2 with the removal of 3;  $\rho_{12}$ ,  $\rho_{13}$ , and  $\rho_{23}$  are the total correlation between variables 1–2, 1–3, and 2–3, respectively. This statistic provides the correlation coefficients between two variables with the exclusion of a third one. Because the partial correlation involves two indices and one variable, for the lag partial correlation calculation, the indices were maintained at the time zero and the variable was lagged.

All correlation coefficients were submitted to a Student's  $t$ -test for a confidence level of 95%, and only the significant correlations were retained for the analyses. The number of degrees of freedom (DOF) was determined by dividing the total time length of the series by the time lag needed to achieve decorrelation time close to zero (Kayano et al., 2009; Servain et al., 2000). The DOFs were determined in each grid point and the lowest value was adopted for all the area, so that the test is the most severe. The DOFs and the respective critical correlations coefficients obtained from the Student's  $t$ -test for each variable are shown in Table 2.

The correlation differences between the cold PDO regime and the warm PDO regime that changed between 1976 and 1977, were calculated for both the total and partial correlations and summarized in correlation maps. To assess the statistical significance of these differences, first a Fisher transformation was applied to the correlation coefficients of each PDO phase using Eq. (4), this operation returns the Fisher's  $z$ -score statistics, then the difference between the  $z$  score of each PDO period was calculated. The Fisher transformation makes the correlation distributions approximately normal.

$$z = \frac{1}{2} [\log_e(1 + \rho) - \log_e(1 - \rho)]. \quad (4)$$

The differences between each pair of  $z$ -score were divided by the estimated Standard Error (SE) of this difference. The SE was found using Eq. (5), where  $n_1$  and  $n_2$  are the DOFs for each PDO period. The correlation difference is significant at a confidence level of 95% only when the absolute value of this division is greater than 1.96.

$$SE = \sqrt{\frac{1}{n_1 - 3} + \frac{1}{n_2 - 3}}. \quad (5)$$

### 3. Results and discussion

#### 3.1. Compounded remote and local forcings in total correlations

Positive correlations between Niño3 and SSTA dominate the tropical South Atlantic roughly centered along the northern limb of the subtropical ocean gyre, and show marked differences between the cold (Fig. 2a) and warm PDO phases (Fig. 2b). The time lag for maximum correlations was 7 months, which compares very well with previous results on the lagged relations between the ENSO and the tropical South Atlantic SST variability (Enfield and Mayer, 1997; Kayano et al., 2012; Lanzante,

**Table 2**

Degrees of freedom (DOFs) and critical correlation values (in parenthesis) at 95% level of confidence for each variable.

Variable	Cold PDO period	Warm PDO period	AAO period
SST	25 (0.38)	27 (0.37)	26 (0.37)
Wind stress	17 (0.45)	25 (0.38)	26 (0.37)
SLP	25 (0.38)	26 (0.37)	26 (0.37)
OLR		24 (0.39)	24 (0.39)

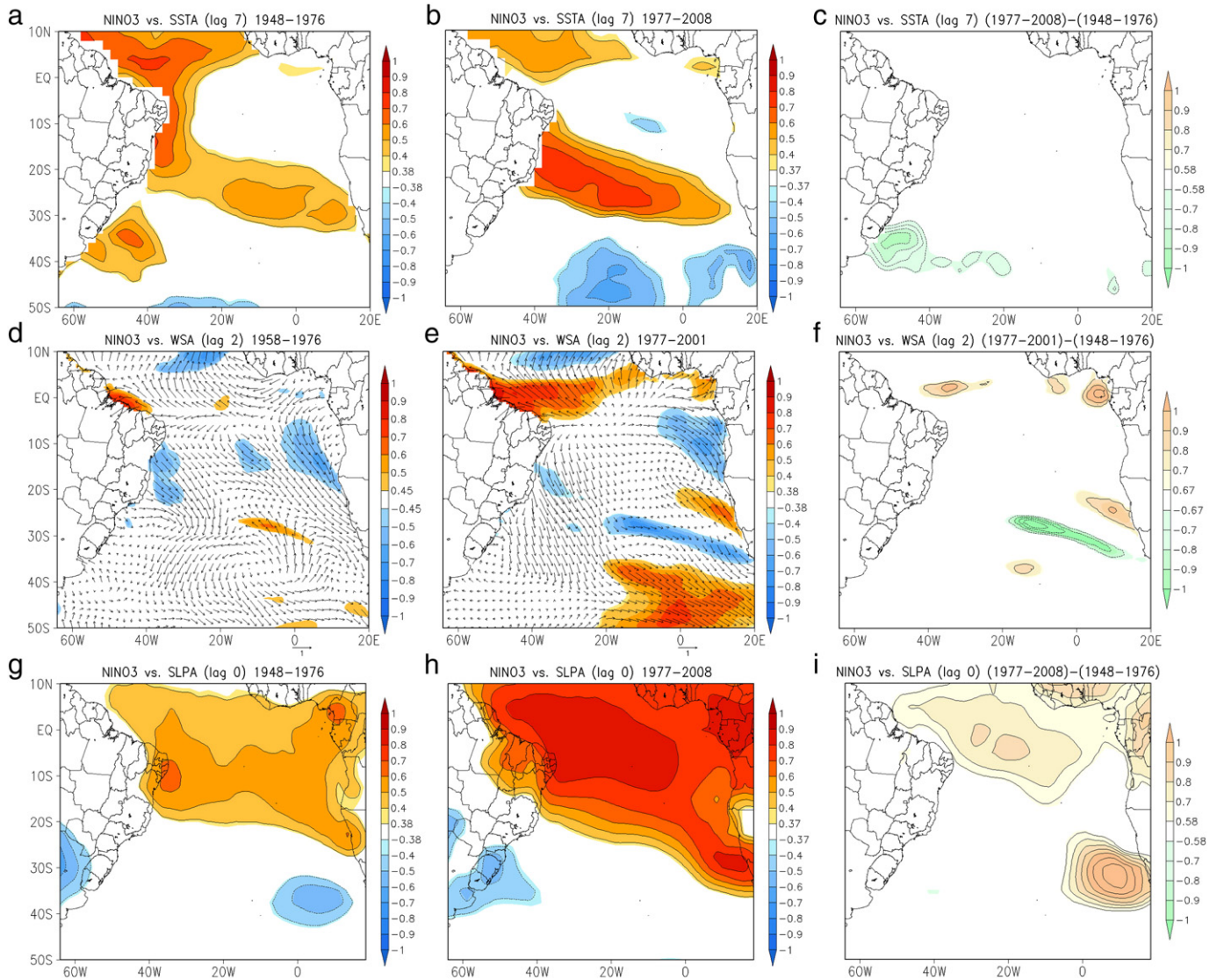


**Fig. 2.** Correlations between Niño3 and the SSTA during the: (a) PDO cold phase; (b) PDO warm phase; (c) difference of correlations shown in (a) and (b). Correlations between Niño3 and WSA during the: (d) PDO cold phase; (e) PDO warm phase; (f) difference of correlations shown in (d) and (e). Correlations between Niño3 and SLPA during the: (g) PDO cold phase; (h) PDO warm phase; (i) difference of correlations shown in (g) and (h). Only the significant correlations are shown in colored shaded. The threshold value above which the absolute correlations are significant is: 0.38 in (a), (e) and (g); 0.37 in (b) and (h); 0.58 in (c) and (i); 0.45 in (d); and 0.67 in (f). The contour interval is 0.1 in (a), (b), (c), (g), (h) and (i) and is 0.2 in (f). Vectors in the WSA maps represent the vectorial sum of correlations in the zonal and meridional directions.

1996). During the cold PDO phase (Fig. 2a), the maximum correlations (0.7) between Niño3 and SSTA are concentrated along the western boundary of the South Atlantic, just north of the equator. During the warm PDO phase this center of high correlations gets weaker and the positive correlations along the northern limb of the subtropical gyre increase from 0.5 to 0.7 (Fig. 2b). Negative correlations in the extratropical South Atlantic of up to  $-0.6$  are much broader during the warm PDO phase (Fig. 2b), than during the cold phase. The correlation map between Niño3 and SSTA during the warm PDO phase has similarities with the southwest South Atlantic SST mode found by Kayano et al. (2012), this work shows that this mode is strongly lagged (two seasons) relative to the ENSO. Overall, positive correlations between Niño3 and SSTA cover all the Brazilian LMEs during the cold PDO phase. Significant correlations (0.5) are noted in the southern Brazil LME only during the cold phase. For both PDO phases, the interpretation is that the areas with positive (negative) correlations experienced an anomalous sea surface warming during an El Niño (La Niña) event and an anomalous sea surface cooling during a La Niña (El Niño) event.

It is possible to argue that the PDO modulates the thermodynamic control of the ocean–atmosphere system that influences the local

SSTAs in the South Brazil LME. This reasoning hinges on the fact that SSTAs over the southwest Atlantic is uncorrelated with Niño3 (Fig. 2g) during the cold PDO phase, but it shows high negative correlations ( $-0.4$  to  $-0.5$ ) during the warm phase (Fig. 2h). In the warm PDO phase, lower (higher) than average SLP over the southwest Atlantic during an El Niño (La Niña) event would increase (reduce) cloudiness and reduce (increase) the net radiative energy input into the ocean, hindering the observed warming (cooling) during El Niño (La Niña) seen in the previous cold phase.

The decadal behavior of the tropical Atlantic SSTAs is largely controlled by anomalous vertical heat transport and heat flux, but in the subtropical South Atlantic, decadal SSTA variability is generated by the surface air–sea heat flux and damped by oceanic heat transport (Tourre et al., 1999; Wu et al., 2004). Note that the significant differences of the ENSO influence on SSTAs in the southwest Atlantic, between the cold and warm PDO regimes (Fig. 2c), give further evidence of a strong ocean–atmosphere coupling. This mechanism has already been hinted at by Soares et al. (2011) as responsible for the high interannual oscillation in the production of the Brazilian sardine.

Correlation maps of Niño3 vs. WSA show high negative values along the coast of Angola, which indicate a weakening (strengthening) of southeasterly trades in the eastern side of the tropical South Atlantic during the El Niño (La Niña) event (Fig. 2d and e). This is more accentuated during the warm PDO phase (Fig. 2e). This contrasts with a zonal band of positive correlations between 5°S and 5°N in the western equatorial side of the basin, where a strengthening (weakening) of the southerlies occurs during an El Niño (a La Niña) event. This feature is also more accentuated during the warm than the cold PDO phase. During the cold PDO phase (Fig. 2d), positive correlations between Niño3 and WSA are restricted to a smaller area in the western equatorial Atlantic, and is confirmed by the significant positive correlation differences between PDO phases shown in Fig. 2f. During the warm PDO phase (Fig. 2e), a large area with positive correlations between Niño3 and WSA is evident in the southeastern South Atlantic between 40°S and 50°S. This is due to the strengthening (weakening) of the westerlies in this area during the El Niño (La Niña) event during the warm PDO phase. There are also two other areas with significant correlations between Niño3 and WSA, one positive off the Namibia coast and to the south of this area, a negative one.

It is evident that the evolution from cold to warm PDO regimes was followed by increased spatial variability of SSTA and WSA, particularly along the western African LMEs. The relative positions of the positive (poleward) and negative (mostly equatorward) correlation areas between Niño3 and WSA, along the coasts of Angola and Namibia, highlight their possible association with the core of Benguela upwelling (the semi-permanent cell centered at 27°S) and the Agulhas Eddy Corridor (AEC), respectively (Grotsky and Carton, 2006; Shannon and Nelson, 1996). This aspect is more evident for the warm PDO phase.

Positive correlations between Niño3 and SLPA (zero lag) are noted in the Atlantic sector between 10°N and 20°S for both PDO phases (Fig. 2g and h). Therefore, under El Niño (La Niña) occurrence, positive (negative) SLPAs are observed in this sector. These correlations are higher during the warm than during the cold PDO phase. During the warm PDO phase, centers of high positive correlation values (0.8) close to the Namibia–Angola border and within a broad region covering most of the tropical South Atlantic, including the Brazilian Nordeste (northeast semi-arid region) are noted. It is plausible to assume that the forcing mechanism in the Benguela environment is related to large scale processes, including a stronger impact of SLPA on the intensity of the oceanic gyre circulation transports (Wainer and Venegas, 2002) during the warm PDO regime. This impact is likely to be of a reduction (an increase) in the intensity of gyre circulation associated with the El Niño (La Niña) during the warm PDO regime, as suggested by the significant negative difference in correlation shown in Fig. 2f. The spatial location of this difference coincides with the average position of the Subtropical (anticyclonic) High Pressure center. Therefore, the atmosphere plays an important role in the modulation of remote forcing in the western Africa LMEs, leading to significant changes in the oceanic regime as seen in the warm-minus-cold PDO difference maps (see Fig. 2f and i).

The inter-hemispheric SST gradient, TSA, TNA modes, and the southern hemisphere annular mode AAO are the local climate modes that account for most of the variance of the tropical and South Atlantic to changes in the coupled local ocean–atmospheric interaction (see Enfield and Mayer, 1997; Enfield et al., 1999). Overall, correlations involving the TNA or the index for the interhemispheric SST gradient were not significant or were lower than those for TSA. Therefore, we will focus on those results involving the local indices TSA and AAO. The highest linear correlation between the TSA and SSTA is found during the cold PDO phase and becomes weaker in the subsequent warm PDO phase (Fig. 3a and b), when the eastern side of the area with significant correlations recedes towards the north and away from the Benguela region.

The significant correlation differences between warm and cold PDO phases are concentrated in the southwestern South Atlantic between 30°S and 40°S for the TSA vs. SSTA (Fig. 3c) and between 30°S and

50°S for the Niño3 vs. SSTA (Fig. 2c). So, the South Brazil LME in the southwest Atlantic and the Benguela Current LME can be considered as special sites, where decadal changes controlled by the PDO regime play a significant role in modulating the influence of both ENSO and TSA, despite differences in the time lag. Along the cold to warm PDO transition, the spatial pattern of the correlations between TSA vs. SSTA (Fig. 3a, b) depicts a more zonal structure. For the warm PDO phase, the positive correlations between the TSA and SSTA are associated with a weakening of the southeast trades in the equatorial western Atlantic (Fig. 3e). This zonal pattern of positive TSA vs. SSTA correlations, concentrated between 20°S and 5°N, is very similar to the Atlantic equatorial mode identified by Zebiak (1993). It should be highlighted that these correlations are antisymmetrical with respect to Niño3 vs. SSTA, particularly during the warm PDO regime (Fig. 2b). This implies that Niño3 and TSA influences on the SSTA occur in nearly complementary areas of the tropical Atlantic. Interannual SSTAs equatorward of 20°S are driven mainly by surface heat flux (Wu et al., 2004) and/or heat content (Ding et al., 2010). This might be the main process behind the influence of TSA on the equatorial Atlantic SSTAs. Note that the linear (negative) relation of TSA vs. WSA between 5°S and 5°N during the PDO warm phase (Fig. 3e) is absent during the PDO cold phase (Fig. 3d) and has an opposite sign of that of Niño3 vs. WSA (compared with Fig. 2e).

The correlation map between TSA and SLPA shows significant negative correlations centered at (30°S, 0°E) for the cold PDO phase and at (20°S, 0°E) for the positive PDO phase. During the positive PDO phase the negative significant correlations between TSA and SLPA extend equatorward. The centers of high correlations (−0.7) between the TSA and SLPA are close to the mean position of the South Atlantic subtropical high. This result suggests that the TSA contribute to alter the South Atlantic subtropical high mean position along the transition from cold to warm PDO regimes (see Fig. 3i). Furthermore, the positive (negative) TSA is associated with reduced (increased) intensity of the South Atlantic subtropical high pressure.

The correlations TSA vs. SLPA (Fig. 3g, h) and Niño3 vs. SLPA (Fig. 2g, h) show opposite signs in the Atlantic sector between 10°N and 20°S, in particular for the warm PDO phase. This is yet another evidence of the competing influences of local and remote processes on the tropical Atlantic. Note that the PDO regime shift induced large scale changes in the relationship between Niño3 and SLPAs in the South Atlantic (Fig. 2i), but only minor and localized changes for TSA (Fig. 3i).

It has been hypothesized that the TNA and TSA modes originate from the local tropical Atlantic system, and that ENSO forcing acts to enhance their variance and modulate their temporal evolution (Wu et al., 2004). If we look at the correlations between Niño3, TNA and OLRA, it becomes clear that these are likely to have a similar influence enhancing surface convergence at the atmospheric boundary layer and cloud formation (Fig. 4a, c). The strong negative (−0.8) correlations between Niño3 and OLRA (Fig. 4a) noted in the southwest Atlantic during the warm PDO (1979–2008) indicate increased (reduced) cloudiness in this region associated with an El Niño (La Niña) event and this pattern is in agreement with the hypothesis that the PDO modulates the thermodynamic control of the SSTA in the South Brazil LME. Numerical experiments with an atmospheric general circulation model (AGCM) and an ocean general circulation model (OGCM) showed a strong relation between reduced incident shortwave radiation due to increased cloudiness and negative SSTAs in the southwest tropical Atlantic (Chaves and Nobre, 2004). The area of negative correlations of TNA vs. OLRA (Fig. 4c) is coincident with a strong cloud forming area called the South Atlantic Convergence Zone (SACZ) (Carvalho et al., 2004; Kodama, 1992), which is predominant in the South Brazil LME. In contrast, the correlation map for the TSA (Fig. 4b) not only shows opposite (negative) sign correlations (compared to those for the Niño3 and TNA) along the equator, but also has a different area of positive correlations away from the equator, between 10°S and 25°S. Reduced intensity of the South Atlantic subtropical high pressure system and reduced inter-hemispheric surface

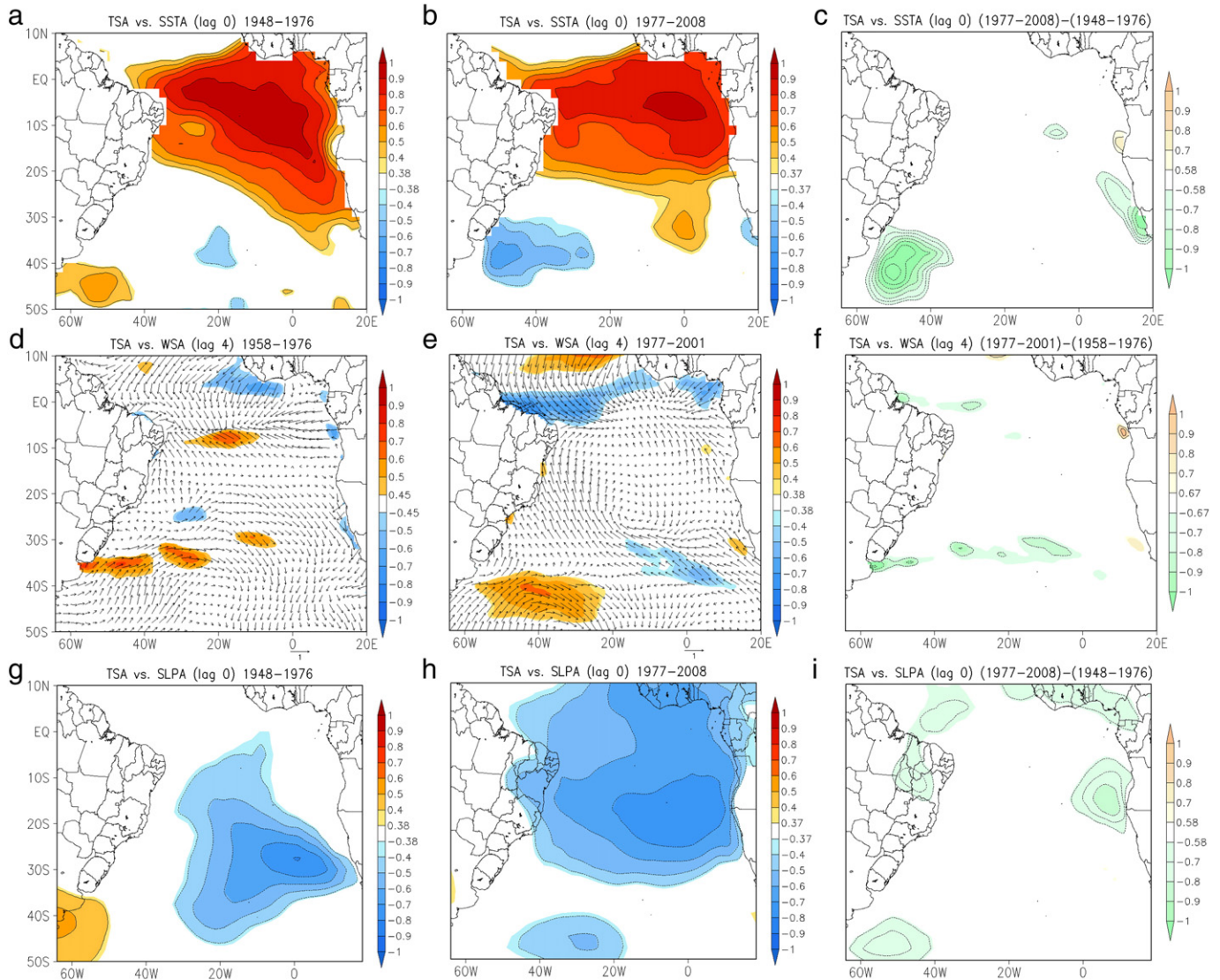


**Fig. 3.** Correlations between TSA and the SSTA during the: (a) PDO cold phase; (b) PDO warm phase; (c) Difference of the correlations shown in (a) and (b). Correlations between TSA and the WSA during the: (d) PDO cold phase; (e) PDO warm phase; (f) Differences of correlations shown in (d) and (e). Correlations between TSA and the SLPA during the: (g) PDO cold phase; (h) PDO warm phase. (i) Difference of the correlations shown in (g) and (h). Display is the same as in Fig. 1. Only the significant correlations are shown and the threshold values above which the absolute correlations are significant are 0.37 in (b) and (h); 0.38 in (a), (e) and (g); 0.47 in (d); 0.58 in (c) and (i); and 0.67 in (f).

heat advection due to the weaker southeasterly trades (Fig. 3e, h), and positive SSTAs between 20°S and 5°N (Fig. 3b) are concurrent with reduced meridional surface Ekman transport (not shown) during the

warm PDO regime. Significant correlation differences between PDO regimes for the TSA vs. WSA centered along the equator and in an area between 30°S and 40°S (Fig. 3f) are in agreement with this mechanism.

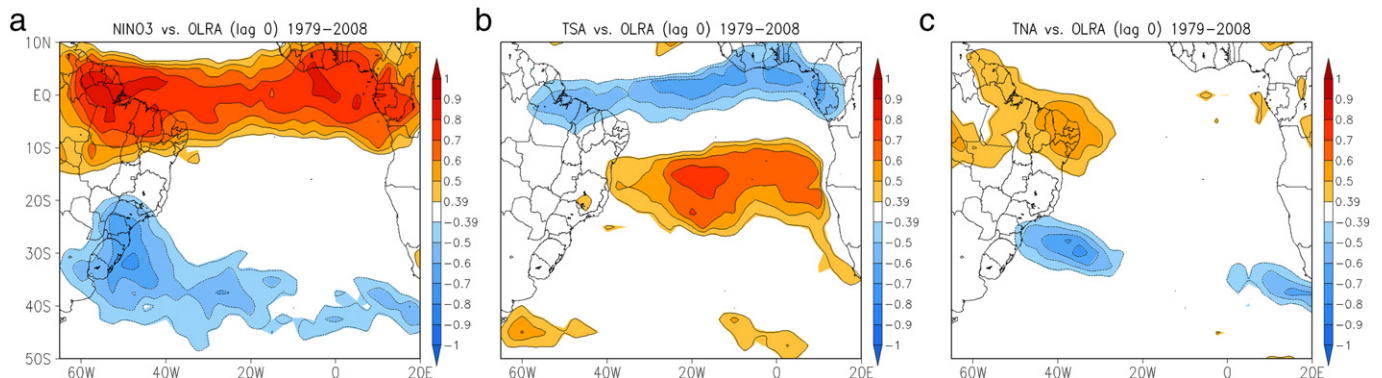


**Fig. 4.** Correlations between and the: (a) Niño3 and OLRA; (b) TSA and OLRA; and (c) TNA and OLRA. Correlation coefficients were calculated only for the PDO warm phase. Only the significant correlations are shown in varying shades of color. The contour interval is 0.1. The threshold value above which the absolute correlations are significant is 0.39 in (a), (b) and (c).

The AAO primary mode of internal atmospheric variability has a strong zonally symmetric character, leading to strong hemispheric-scale synchronization with ocean variability that enhances atmosphere–ocean covariability (Hall and Visbeck, 2002). As a predominant component of the southern hemisphere internal mode, the AAO plays an important role in both the Brazilian and west African LMEs via the Pacific–South American teleconnection (Ding et al., 2012; Karoly, 1989). Its effect on the SSTAs are widespread, positive (0.5) zonal correlations are found around 5°S, between 40°S and 50°S. There is also an important negative correlation (−0.6) on the South Brazil LME between 25°S and 35°S (Fig. 5a), coincident with the position of the oceanic branch of the SACZ. Results of a coarse-resolution coupled ocean–atmosphere model (Hall and Visbeck, 2002) showed that positive AAO is correlated with a reduction of poleward heat transport at about 50°S, and an increase around 30°S. This agrees well with our results that point to positive correlations between AAO and SSTAs where meridional heat transport is reduced and negative correlations where it increases, along the western side of the basin. Negative correlations of AAO vs. WSA (Fig. 5b) and ETA (Fig. 5c), between 40°S and 50°S, also agree with the above mechanism, although mostly concentrated eastward of 20°W. The expected effect on the regional heat budget is also confirmed by the increased OLRA for the positive AAO (Fig. 5d), that spreads across the basin south of 40°S. According to Hall and Visbeck (2002), the poleward migration of the jet stream would lead to a reduction in baroclinic activity and rising motion, hence reduced cloud formation. We have, indeed, detected a broad zonally oriented region of high positive OLRA vs. AAO correlation along a latitudinal band between 40°S and 50°S (Fig. 5d).

### 3.2. Interactions between remote and local forcings in partial correlations

The analysis of partial correlation maps focus on the relative importance of local and remote forcings on the climate variability of the South Atlantic LMEs. Prior to the analyses of the partial correlation maps, the correlations among every two indices involved in the partial correlations are presented in Table 3. The Niño3 and TSA are weakly and positively correlated during the cold PDO phase and significantly and negatively correlated during the warm PDO phase. The larger magnitude of the correlation for the warm than for the cold PDO phase might lead to a stronger effect when TSA is removed during the warm than during the cold PDO phase. The Niño3 and TNA are positively correlated in both phases of the PDO, with nearly comparable correlation magnitudes. However, only the correlation for the cold PDO phase is significant. The AAO is weakly and negatively correlated with Niño3 and with TNA, and significantly and positively correlated with TSA.

Removing the influence of TSA on the relation between ENSO and SSTAs in the South Atlantic slightly increases the positive correlations, during both the cold (Fig. 6a) and warm (Fig. 6b) PDO regimes (compare with Fig. 2a and b). During the warm PDO regime, TSA acted to reduce the influence of ENSO on SSTAs along the North and East Brazil LMEs and on the Guinea Current LME. From a statistical point of view, this is caused by the fact that the TSA and Niño3 are negatively (and significantly) correlated (see Table 3). A physical explanation can be found in Wu et al. (2004), whereby the ENSO modulates the behavior of TSA by enhancing SSTA variance, possibly via changes in surface heat flux. The authors used a modeling experiment called partial coupling, with

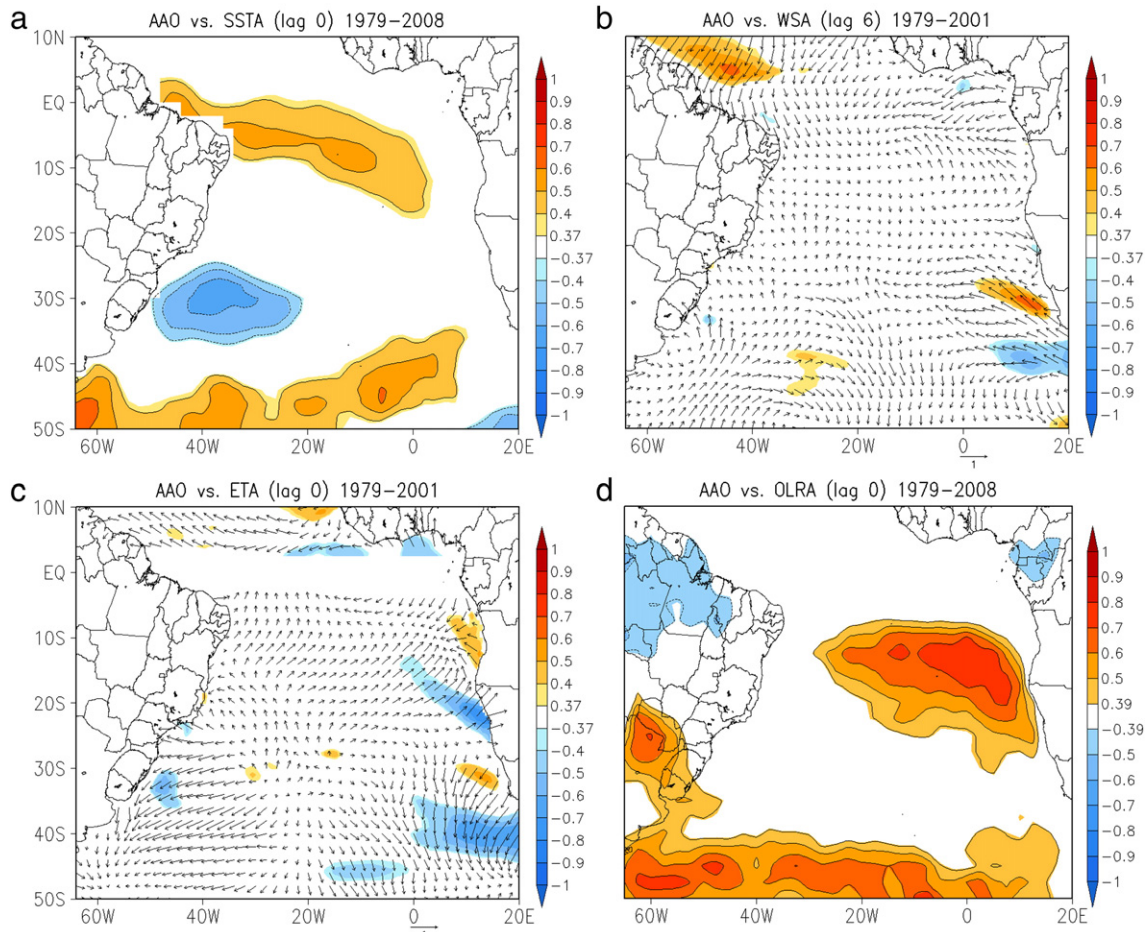


**Fig. 5.** Correlations between: (a) AAO and SSTA; (b) AAO and WSA; (c) AAO and ETA; (d) AAO and OLRA. Only the significant correlations are shown in varying shades of color. The threshold value above which the absolute correlations are significant is 0.37 in (a), (b) and (c), and 0.39 in (d). The contour interval is 0.1 in (a) and (d). Only the significant correlations are shown in varying shades of color. Vectors in the WSA and ETA maps are as in Fig. 1. Correlation coefficients were calculated only for the PDO warm phase.

**Table 3**

Correlations between indices for the indicated periods. The significant correlations at the 95% confidence level are indicated with an asterisk.

Indices	Cold PDO period	Warm PDO period
Niño3 × TSA	0.16	−0.34*
Niño3 × TNA	0.47*	0.31
Niño3 × AAO		−0.15
AAO × TSA		0.38*
AAO × TNA		−0.12

a prescribed annual cycle of SST, to show that ENSO dictates the interannual variability of the TSA (and TNA). However, fixed SST boundary conditions cause thermodynamic damping and tend to underestimate atmospheric stochastic variability.

It seems that the influence of TSA on the relation of Niño3 vs. SSTA did not change between different PDO regimes (Fig. 6c). The correlation differences are very similar to the total correlation difference map shown in Fig. 2c. The removal of TNA from the Niño3 vs. SSTA relation (Fig. 6d, e) causes a slight reduction in correlations along the North and East Brazil LMEs compared to total correlations. Significant differences between PDO phases appear in small patches of the central and northeast sectors of the South Atlantic (Fig. 6f). These are not seen in the differences between total correlations (Fig. 2c). Our results are in accordance with the view of a stronger ENSO connection in the North Atlantic, which seems to be particularly strong in the multi-decadal band (Enfield and Mayer, 1997; Enfield et al., 1999).

Although the maps of the correlation difference between the warm and cold PDO phases for the total (Niño3 vs. WSA) (Fig. 2f) and partial correlations (Niño3 vs. WSA-TSA) (Fig. 7c) are very similar, the removal of the TSA (Figs. 7a, b) from the correlations between Niño3 vs. WSA caused impact. This is particularly noticeable in the Guinea Current LME where the weakening of the southeasterly vectors is more accentuated for the partial correlation map during the cold PDO phase

(compare Figs. 2d, 7a). Another area where the removal of the TSA from the correlation between Niño3 and WSA caused impact is the East Brazil LME, where northerly and northwesterly wind stress enhanced during both PDO phases (compare Figs. 2d and 7a, and compare Figs. 2e and 7b). Also, magnitudes of the vectors of the partial correlation map (Niño3 vs. WSA-TSA) are larger than those of the total correlation (Niño3 vs. WSA) in particular in western South Atlantic between 5°S and 40°S. This is more conspicuous for the warm PDO phase.

The maps of the correlation difference between warm and cold PDO phases for the total (Niño3 vs. WSA) (Fig. 2f) and partial correlations (Niño3 vs. WSA-TNA) (Fig. 7f) are very similar. However, the removal of the TNA (Fig. 7d, e) from the correlations between Niño3 vs. WSA caused in general a strengthening of the vector magnitudes for both PDO phases. Indeed, the removal of the TNA causes a broadening of the area where the southeasterly vectors are weakened and the strengthening of the northwesterly vectors in the East Brazil LME during the cold PDO regime (Fig. 7d). In addition, the northerly and northwesterly vectors are strengthened in the western South Atlantic between 10°S and 40°S, during the warm phase (Fig. 7e). Since Niño3 and TNA are highly correlated (Table 3), removing the influence of the latter on the Niño3 vs. WSA relationship enhanced the ENSO signal seen in Fig. 2d and e, pointing towards a significant basin-scale control (damping) of the Atlantic ocean–atmosphere system on the remote influence of ENSO on an interannual timescale.

Removing the influence of TSA on Niño3 vs. SLPA correlations (Fig. 8a, b and c) the maximum positive correlations slightly increase from 0.5 to 0.6 along the tropical South Atlantic during the cold PDO, but no significant effect is noted during the warm phase (Fig. 8b). The most evident change is the broadening of the negative correlation region in higher latitudes (Fig. 8b) during the warm PDO phase. This is where the removal of the TSA influences most between both phases (Fig. 8c), when compared to the total correlation field (Fig. 2i). There is a significant drop in the differences of correlation between warm and cold PDO in the tropical Atlantic, with the removal of the influence

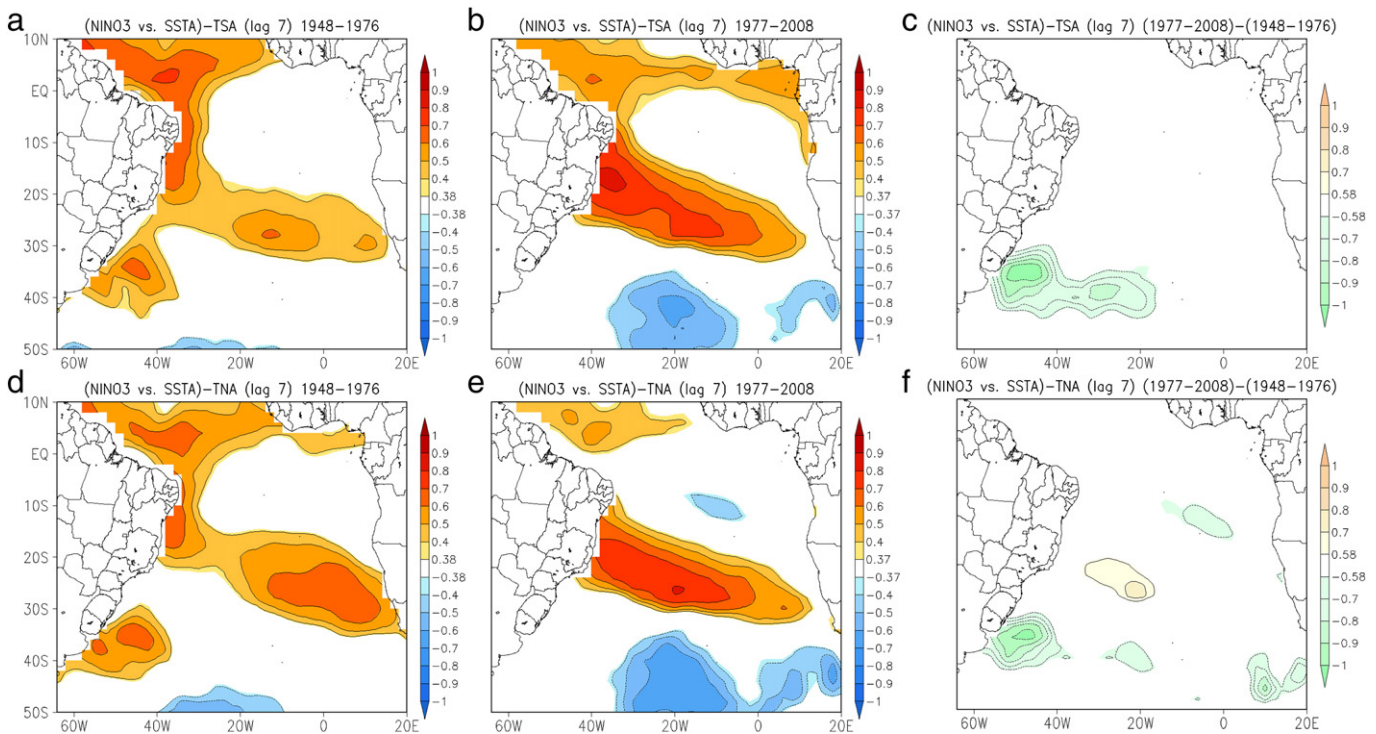


**Fig. 6.** Partial correlations between Niño3 and SSTA minus TSA during the: (a) PDO cold phase; (b) PDO warm phase (b); (c) differences of the partial correlation shown in (a) and (b). Partial correlations between Niño3 and SSTA minus TNA during the: (d) PDO cold phase; (e) during the PDO warm phase; (f) differences of the partial correlations shown in (d) and (e). Only the significant correlations are shown in varying shades of color. The threshold value above which the absolute correlations are significant is 0.38 in (a) and (d), 0.37 in (b) and (e), and 0.58 in (c) and (f).

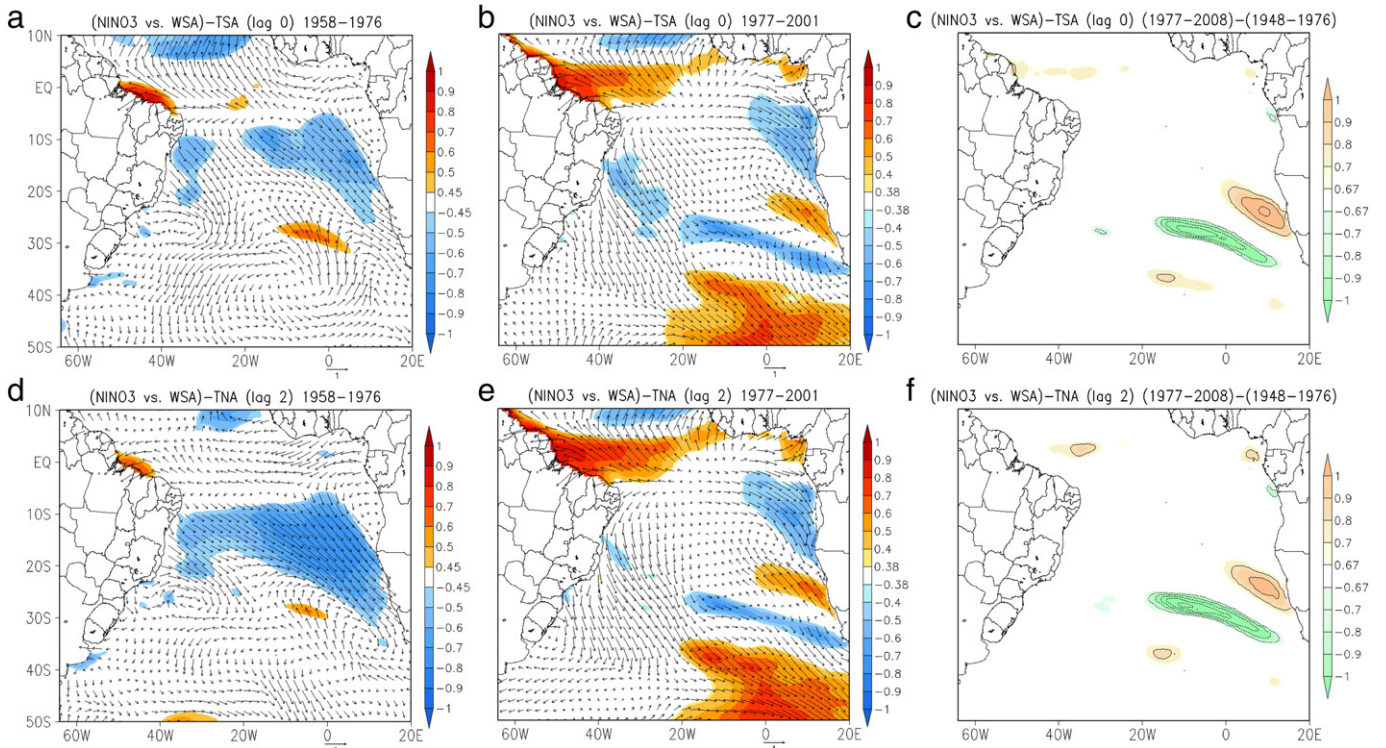


**Fig. 7.** Partial correlations between Niño3 and WSA minus TSA during the: (a) PDO cold phase; (b) PDO warm phase; (c) Differences of the partial correlations shown in (a) and (b). Partial correlations between Niño3 and WSA minus TNA during the: (d) PDO cold phase; (e) PDO warm phase; (f) differences of the partial correlations shown in (d) and (e). Vectors in the WSA maps are as in Fig. 1. The contour interval is 0.2 in (c) and (f). Only the significant correlations are shown in varying shades of color. The threshold value above which the absolute correlations are significant is 0.45 in (a) and (d), 0.38 in (b) and (e), and 0.67 in (c) and (f).

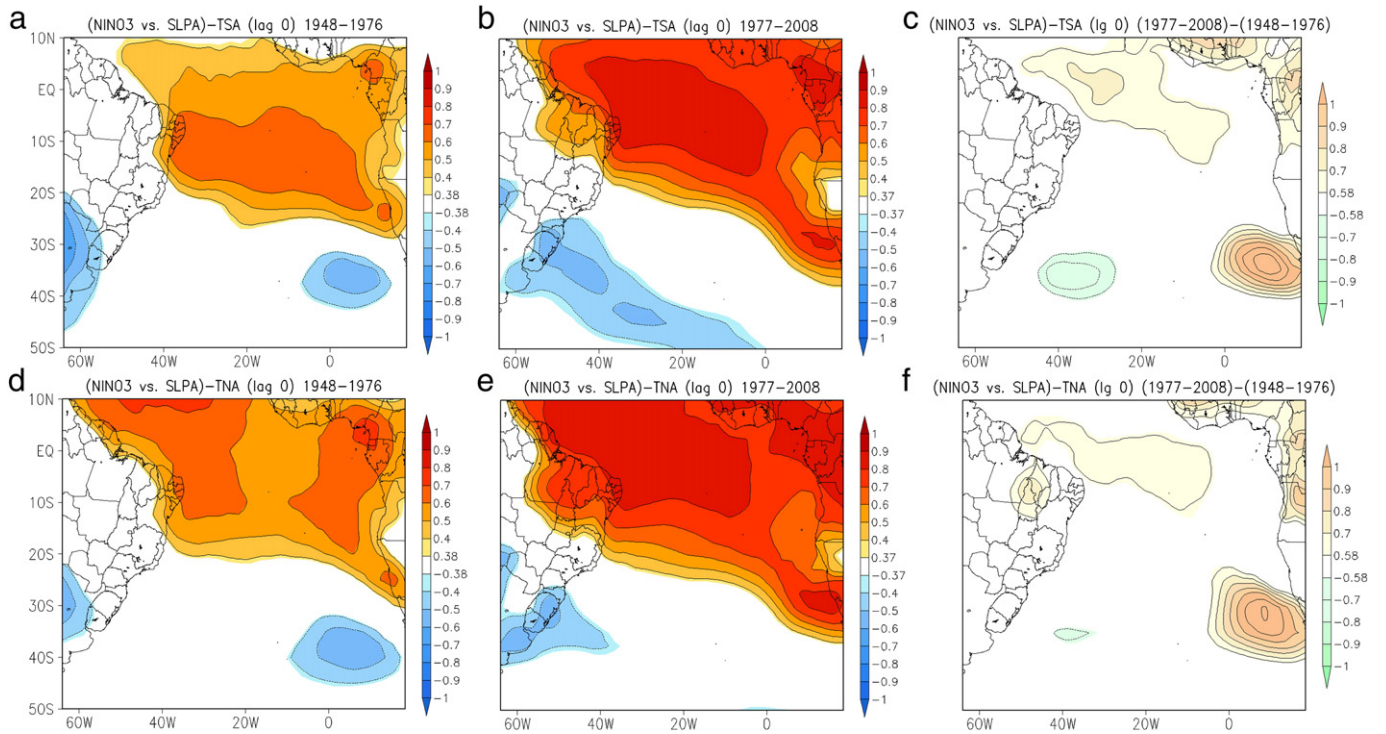


**Fig. 8.** Partial correlations between Niño3 and SLPA minus TSA during the: (a) PDO cold phase; (b) PDO warm phase; (c) difference of the partial correlations shown in (a) and (b). Partial correlations between Niño3 and SLPA minus TNA during the: (d) PDO cold phase; (e) PDO warm phase. (f) Difference of the partial correlations shown in (d) and (e). The contour interval is 0.1 in (a), (b), (c), (d), (e) and (f). Only the significant correlations are shown in varying shades of color. The threshold value above which the absolute correlations are significant is 0.38 in (a) and (d), 0.37 in (b) and (e), and 0.58 in (c) and (f).

of TNA on the Niño3 vs. SLPA (Fig. 8f) due to the increase in correlation during the cold regime (Fig. 8d) and the maintenance of correlation values during the warm regime (Fig. 8e), compared to the total correlations (Fig. 2g, h).

As expected, the removal of the influence of Niño3 (Fig. 9a) and TNA (not shown) from the AAO vs. SSTA total correlations (Fig. 5a) did not affect much the spatial pattern of correlations, or their values (positive and negative). This is in part because the AAO is weakly correlated with the Niño3 and with TNA (Table 3). These results highlight the role of AAO as a predominant component of the southern hemisphere internal mode with a major zonal positive influence on the SSTA between 40°S and 50°S and an inverted (negative) influence on the South Brazil LME. On the other hand, the removal of the TSA (Fig. 9b) modulates the influence of AAO in the tropical Atlantic by reducing its influence on the SSTA, and increasing the positive correlations in higher latitudes. The removal of the influence of Niño3 (Fig. 9c) and TSA from the AAO vs. WSA (Fig. 9d), follows the same pattern described above, where the TSA has a weakening effect on the intensification of the westerly circumpolar winds, and to a lesser extent, on the wind divergence in the Benguela system (Fig. 9d).

The stronger modulation effect of TSA on the AAO, compared to Niño (Fig. 9e and f), is expressed in the radiative energy balance associated to the OLRAs. It is more evident between 10°S and 25°S as a reduction of positive correlation coefficients and their spatial coverage on the Benguela Current LME (compare Fig. 9f and 5d). A small, but significant, area of negative correlations not seen in the total AAO vs. OLRA appears on the East Brazil LME centered at 25°S, in the northern limit of the oceanic SACZ. Carvalho et al. (2004) suggested that the interannual activity of the oceanic SACZ is intensified during warm ENSO events, but our results also point towards a significant modulation of the TSA.

### 3.3. Linking climate variability and the functioning of LMEs in the South Atlantic

There is an increasing body of evidence that associate environmental changes driven by climate variations with biological regime shifts in LMEs (Wang et al., 2010). It may seem counterintuitive, but changes in biological regimes tend to be identified before one is able to present a proper explanation of the physical processes responsible for these changes. One such example is the mid-seventies PDO shift, that resulted in a shift from the anchovy dominated regime to the sardine dominated regime in the Pacific (Chavez et al., 2003). Despite the typically short length of biological time series, there are clear evidences of interannual changes in the pelagic ecosystems of the South Atlantic. The interannual variability of egg concentration of the Brazilian sardine in the South Brazil LME was interpreted as a response to the expansion and contraction of the spawning habitat (Gigliotti et al., 2010). During periods of spawning habitat expansion, the SSTAs were zero or slightly negative, whereas for the contraction period anomalies were all positive. If we focus our analysis only on the oceanic conditions, it becomes apparent that suitable spawning sites could be provided by the entrainment of the colder and less saline South Atlantic Central Water (SACW) onto the shelf due to the combined effect of coastal wind-driven and meander-induced upwelling. Looking at the ocean–atmosphere system however, Soares et al. (2011) found that the Brazilian sardine catch maxima occurs one year after episodes of increased cloud cover and reduced incidence of shortwave radiation that cools down summertime SSTA along the East Brazilian LME. In contrast, sardine catch minima occurred one year after warmer SSTA conditions concurrent with a less intense South Atlantic Convergence Zone. The above evidence indicates that the spatial structure of the spawning habitat of the Brazilian sardine is influenced by specific ocean–atmosphere interactions rather than

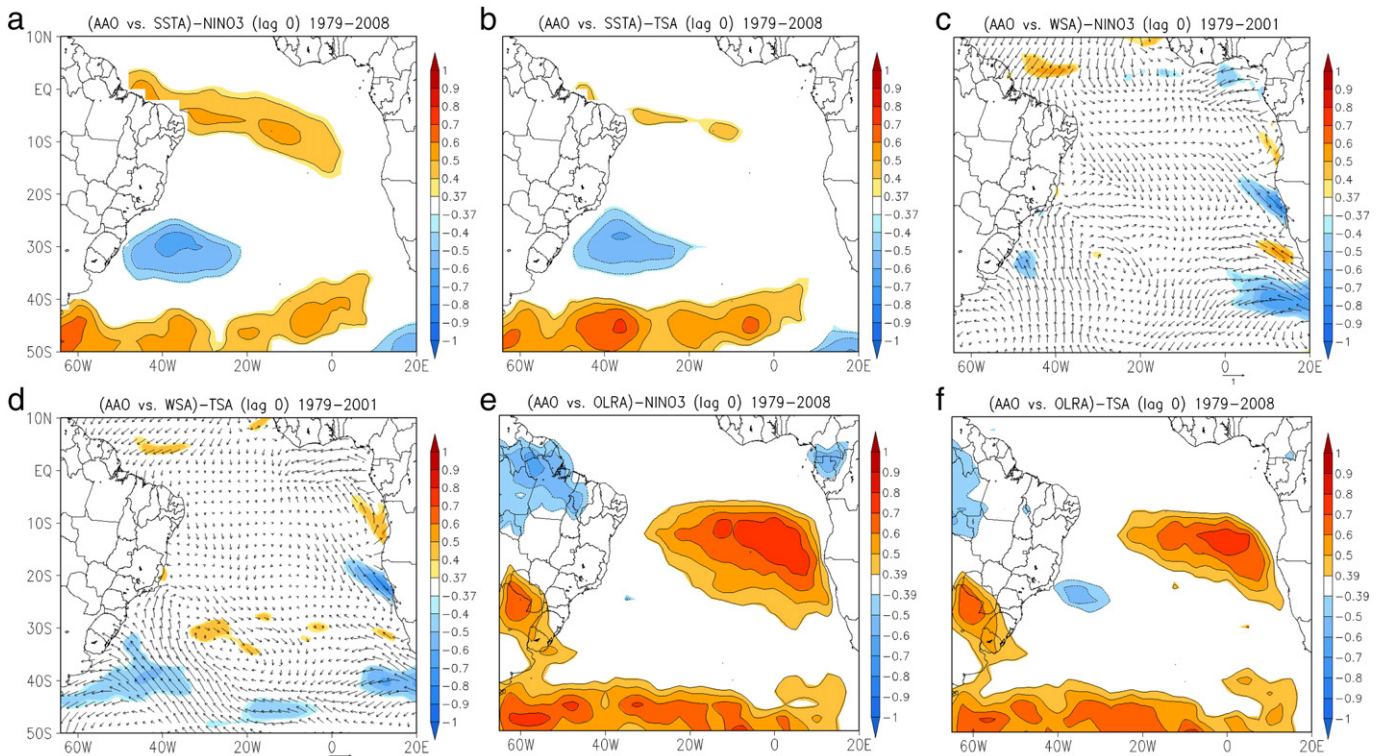


**Fig. 9.** Partial correlations between: (a) AAO and SSTA minus Niño3; (b) AAO and SSTA minus TSA; (c) AAO and WSA minus Niño3; (d) AAO and WSA minus TSA; (e) AAO and OLRA minus Niño3; (f) AAO and OLRA minus TSA. Vectors in the WSA maps are as in Fig. 1. The contour interval is 0.1 in (a), (b), (e) and (f). Only the significant correlations are shown in varying shades of color. The threshold value above which the absolute correlations are significant is 0.37 in (a), (b), (c) and (d), and 0.39 in (e) and (f).

simply as a result of a physically stable environment. This climatic constraint strongly affects the interannual variability of the Brazilian sardine production (Soares et al., 2011).

Recently, warming trends of SST were detected in most global datasets and have shown that the largest trends are found in the middle latitudes of both hemispheres (Deser et al., 2010). This is where the dominant local South Atlantic mode and remote forcings tend to show significant decadal changes, resulting in complex climate regime shifts. Alheit and Bakun (2010) summarized some important evidence of the linkages between Pacific and Atlantic Oceans, such as the outburst of snipefish (*Macrorhamphosus scolopax* and *M. gracilis*) off the coast of Morocco, and triggerfish in the Gulf of Guinea following the temporary demise of the sardine (*Sardinella aurita*) population. These events involved complex pelagic wasp-waist pelagic control (species at intermediate trophic level controls the energy flux from low and also provides the energy for high trophic levels) and disrupted local fishing operations with serious impacts on local economies. They have concluded that remote and local forcings act together to produce specific patterns of variations in the climate-fisheries system, and that simple empirical relationships are likely to be misleading (see also Wang et al., 2010). It has also been suggested that future fish production may increase in high latitude regions following local warming and reduced ice cover, or decline in low-latitude regions due to increased static stability of the water column that reduce vertical mixing and recycling of nutrients (Brander, 2007).

There is an opposite trend between the sardine (*Sardinops sagax*) and anchovy (*Engraulis capensis*) landings in the southern portion of the Benguela Current LME. It is worth noting that in the south of the Benguela Current LME the influence of ENSO is stronger, while that to the north the influence of the Benguela Niño is more evident (Boyd et al., 1998). The correlation analyses show that the Niño3 is positively correlated with a southeast WSA in the south of the Benguela Current LME during the warm PDO phase (Fig. 2e). Boyd et al. (1998) have associated anchovy recruitment number failures that occurs in the southern Benguela Current LME due to advective losses (eggs and larvae) with periods of southeast strong winds coinciding with El Niño events. In this way, it is possible to suggest that failure in the anchovy recruitment in the Benguela Current LME is related to stronger southeast winds in the south Benguela Current LME in the El Niño events during the warm PDO phase. Shannon et al. (2004) discuss that the variability of sardine and anchovy stocks have interannual and interdecadal oscillations. So, evidence points towards the necessity of understanding how different temporal patterns of oscillation interact to influence biological processes through environmental perturbations.

Alheit and Bakun (2010) discussed the association between ENSO and the collapse of sardine (*S. aurita*) followed by high of triggerfish (*Balistes capricus*) in the Guinea Current LME region. These authors suggested that the enhancement of the Walker cell in the equatorial Atlantic during El Niño years cause an intensification of the trade winds, leading to an intense upwelling in the Guinea Gulf. The increased persistence of cold waters would explain the increase in sardine landings. The end of the El Niño causes a disruption of the Walker cell, warming the surface waters and causing the collapse of sardine fisheries. The correlation analysis between Niño3 and SSTA showed positive correlation during the warm PDO in the Gulf Guinea region (Fig. 2b). This correlation is stronger when the influence of the TSA is removed in the partial correlations (Fig. 6b), indicating that positive SSTA in the TSA region dampens the El Niño influence on SSTA in the Guinea Gulf region. We contend that these interactions between remote and local climate modes need to be properly understood so that an accurate connection between climate changes and biological dynamics can be established.

So, it is clear that to promote ecosystem-based management on a spatial scale typical of the LMEs, we need to acquire a minimum level of understanding of how local ocean-atmosphere dynamics interact with remote-forced climatic regimes. Only then, can one filter out the

internal variability from human-induced trends to develop management and adaptation strategies for fishery management devised to mitigate anthropogenic impacts.

#### 4. Conclusions

In this study we present evidence for significant climate regime shifts affecting South Atlantic LMEs based on widely accepted proxies of remote and local forcings on a basin scale. This is strongly modulated by competing influences between local and remote processes acting on the tropical Atlantic. Significant basin-scale control of the ocean-atmosphere system on the interannual remote influence on the South Atlantic is associated to the heat budget, including surface heat flux and oceanic heat transport. Therefore, we contend that by removing atmosphere and ocean trends of our analysis and concentrating on the interannual to decadal climate variability, we can offer a balanced account of the interplay between Pacific (remote) and Atlantic (local) modes on the LMEs of the South Atlantic.

It is noticeable that the differences between the PDO phases on the correlation patterns are more accentuated than those observed when the local influences are removed. So, there is a strong PDO influence on the remote climate driven mechanisms for the oceanic and atmospheric South Atlantic variability. This is particularly conspicuous for the ENSO relationship with the ocean-atmosphere system in South Atlantic. We also highlight that LMEs, as they are presently delimited along the Brazilian and western African coast, may not coherently respond to global climate changes, due to the complex spatial nature of oceanic and atmospheric variability presented here. The evolution from cold to warm PDO regimes was followed by a much higher spatial complexity of the environmental conditions along the western African LMEs.

Although we acknowledge that LMEs are an important tool for environmental-based management actions, their use to monitor the impacts of climate change on marine populations should be taken with caution (cf. Sherman et al., 2009). It is clear that, as far as their dependence on SSTA is concerned, productivity and trophic relations in each of the South Atlantic LMEs are likely to generate mixed responses at the ecosystem level. This could, in turn, induce policy makers to react to a confounded scenario of environmental change.

#### Acknowledgements

The authors thank the support provided by the National Institute of Science and Technology for Climate Changes - Coastal Zones and Atlantic Carbon Experiment (ACEX-CNPq) 558108/ 2009-1. Computational help by Mr. Cristiano P. Oliveira and Mr. Carlos Frederico Bastarz is also acknowledged. The first author is funded by a fellowship from CAPES no. 918572. Luciano Ponzzi Pezzi acknowledges support from CNPq, as a contribution for the PQ (CNPq) project number 304633/ 2012-7. Significant improvements to the manuscript were provided by the helpful comments of Dr. Kenneth Sherman.

#### References

- Alexander, M.A., Bladé, I., Newman, M., Lanzante, J.R., Lau, N.-C., Scott, D.J., 2002. The atmospheric bridge: the influence of ENSO teleconnections on air-sea interaction over the global oceans. *J. Clim.* 15, 2204-2231.
- Alheit, J., Bakun, A., 2010. Population synchronies within and between ocean basins: apparent teleconnections and implications as to physical-biological linkage mechanisms. *J. Mar. Syst.* 79, 267-285.
- Andreoli, R.V., Kayano, M.T., 2003. Evolution of the equatorial and dipole modes of the sea surface temperature in the Tropical Atlantic at decadal scale. *Meteorog. Atmos. Phys.* 83, 277-285. <http://dx.doi.org/10.1007/s00703-002-0568-4>.
- Belkin, I.M., 2009. Rapid warming of large marine ecosystems. *Prog. Oceanogr.* 81, 207-213.
- Boyd, A.J., Shannon, L.J., Shülein, F.H., Taunton-Clark, J., 1998. Food, transport and anchovy recruitment in the southern Benguela upwelling system off South Africa. In: Durand, M.-H., Cury, P., Mendelssohn, R., Roy, C., Bakun, A., Pauly, D. (Eds.), *Global versus Local Changes in Upwelling Systems*. Collection Colloques et Séminaires. ORSTOM, Paris, pp. 195-209.

- Brander, K.M., 2007. Global fish production and climate change. *Proc. Natl. Acad. Sci.* 104, 19709–19714.
- Carvalho, L.M., Jones, C., Liebmann, B., 2004. The South Atlantic Convergence Zone: intensity, form, persistence, and relationships with intraseasonal to interannual activity and extreme rainfall. *J. Clim.* 17, 88–108.
- Chang, P., Fang, Y., Saravanan, R., Ji, L., Seidel, H., 2006. The cause of the fragile relationship between the Pacific El Niño and the Atlantic Niño. *Nature* 443, 324–328.
- Chaves, R.R., Nobre, P., 2004. Interactions between the South Atlantic Ocean and the atmospheric circulation over South America. *Geophys. Res. Lett.* 31, 1–4.
- Chavez, F.P., Ryan, J., Lluch-Cota, S.E., Niquen, M.C., 2003. From anchovies to sardines and back: multidecadal change in the Pacific Ocean. *Science* 299, 217–221.
- Chiang, J.C.H., Lintner, B.R., 2005. Mechanisms of remote tropical surface warming during El Niño. *J. Clim.* 18, 4130–4149.
- Deser, C., Phillips, A.S., Alexander, M.A., 2010. Twentieth century tropical sea surface temperature trends revisited. *Geophys. Res. Lett.* 37, L10701. <http://dx.doi.org/10.1029/2010GL043321>.
- Ding, H., Keenlyside, N.S., Latif, M., 2010. Equatorial Atlantic interannual variability: Role of heat content. *J. Geophys. Res.* 115. <http://dx.doi.org/10.1029/2010JC006304>
- Ding, A., Steig, E.J., Battisti, D.S., Wallace, J.M., 2012. Influence of the tropics on the Southern Annular Mode. *J. Clim.* 25, 6330–6348.
- Enfield, D.B., Mayer, D.A., 1997. Tropical Atlantic SST and its relation to El Niño–Southern Oscillation. *J. Geophys. Res.* 102, 929–945.
- Enfield, D.B., Mestas-Núñez, A.M., Mayer, D.A., Cid-Serrano, L., 1999. How ubiquitous is the dipole relationship in tropical Atlantic sea surface temperature? *J. Geophys. Res.* 104, 7841–7848.
- Giannini, A., Saravanan, R., Chang, P., 2004. The preconditioning role of tropical Atlantic variability in the development of ENSO teleconnection: implications for the prediction of Northeast rainfall. *Clim. Dyn.* 22, 839–855.
- Gigliotti, E.S., Gherardi, D.F.M., Paes, E.T., Katsuragawa, M., 2010. Spatial analysis of egg distribution and geographic changes in the spawning habitat of the Brazilian sardine *Sardinella brasiliensis*. *J. Fish Biol.* 77, 2248–2267.
- Gong, D., Wang, S., 1999. Definition of Antarctic oscillation index. *Geophys. Res. Lett.* 26, 459–462.
- Grodsky, S.A., Carton, J.A., 2006. Influence of the tropics on the climate of the South Atlantic. *Geophys. Res. Lett.* 33, L06719. <http://dx.doi.org/10.1029/2005GL025153>.
- Hall, A., Visbeck, M., 2002. Synchronous variability in the southern hemisphere atmosphere, sea ice, and ocean resulting from the annular mode. *J. Clim.* 15, 3043–3057.
- Hastenrath, S., 1976. Variations in low-latitude circulation and extreme climatic events in the tropical Americas. *J. Atmos. Sci.* 33, 202–215.
- Hastenrath, S., 2006. Circulation and teleconnection mechanisms of Northeast Brazil droughts. *Prog. Oceanogr.* 70, 407–415.
- Kalnay, E., Kanamitsu, M., Kistler, R., Collins, W., Deaven, D., Gandin, L., Iredell, M., Saha, S., White, G., Woollen, J., Zhu, Y., Chelliah, M., Ebisuzaki, W., Higgins, W., Janowiak, J., Mo, K.C., Ropelewski, C., Wang, J., Leetmaa, A., Reynolds, R., Jenne, R., Joseph, D., 1996. The NCEP/NCAR 40-year reanalysis project. *Bull. Am. Meteorol. Soc.* 77, 437–470.
- Karoly, D.J., 1989. Southern Hemisphere circulation features associated with El Niño–Southern Oscillation events. *J. Clim.* 2, 1239–1252.
- Kayano, M.T., Rao, V.B., Moura, A.D., 1988. Tropical circulations and the associated rainfall anomalies during two contrasting years. *Int. J. Climatol.* 8, 477–488.
- Kayano, M.T., Oliveira, C.P., Andreoli, R.V., 2009. Interannual relations between South American rainfall and tropical sea surface temperature anomalies before and after 1976. *Int. J. Climatol.* 29, 1439–1448. <http://dx.doi.org/10.1002/joc.1824>.
- Kayano, M.T., Andreoli, R.V., Souza, R.A.F., 2012. Relations between ENSO and the South Atlantic SST modes and their effects on the South American rainfall. *Int. J. Climatol.* <http://dx.doi.org/10.1002/joc.3569>.
- Kidson, J.W., 1988. Interannual variations in the Southern Hemisphere circulation. *J. Clim.* 1, 1177–1198.
- Kodama, Y., 1992. Large-scale common features of subtropical precipitation zones (the Baiu Frontal Zone, the SPCZ, and the SACZ). Part I: characteristics of subtropical frontal zones. *J. Meteorol. Soc. Jpn* 70, 813–841.
- L'Heureux, M.L., Thompson, D.W.J., 2005. Observed relationships between the El Niño–Southern Oscillation and the extratropical zonal-mean circulation. *J. Clim.* 19, 276–287.
- Lanzante, J.R., 1996. Lag relationships involving tropical sea surface temperatures. *J. Clim.* 9, 2568–2578.
- Liebmann, B., Smith, C.A., 1996. Description of a complete (interpolated) outgoing longwave radiation dataset. *Bull. Am. Meteorol. Soc.* 77, 1275–1277.
- MacDonald, G.M., Case, R.A., 2005. Variations in the Pacific Decadal Oscillation over the past millennium. *Geophys. Res. Lett.* 32, L08703. <http://dx.doi.org/10.1029/2005GL022478>.
- Mantua, N.J., Hare, S.R., 2002. The Pacific decadal oscillation. *J. Oceanogr.* 58, 35–44.
- Mantua, N.J., Hare, S.R., Zhang, Y., Wallace, J.M., Francis, R.C., 1997. Pacific inter-decadal climate oscillation with impacts on salmon production. *Bull. Am. Meteorol. Soc.* 78, 1069–1079.
- Moura, A.D., Shukla, J., 1981. On the dynamics of droughts in Northeast Brazil: Observations, Theory and Numerical Experiments with a General-Circulation Model. *J. Atmos. Sci.* 38, 2653–2675.
- Nobre, P., Shukla, J., 1996. Variations of sea surface temperature, wind stress, and rainfall over the tropical Atlantic and South America. *J. Clim.* 9, 2464–2479.
- Overland, J.E., Alheit, J., Bakun, A., Hurrell, J.W., Mackas, D.L., Miller, A.J., 2010. Climate controls on marine ecosystems and fish populations. *J. Mar. Syst.* 79, 305–315.
- Pezzi, L.P., Cavalcanti, I.F.A., 2001. The relative importance of ENSO and tropical Atlantic sea surface temperature anomalies for seasonal precipitation over South America: a numerical study. *Clim. Dyn.* 17, 205–212.
- Servain, J., Wainer, I., Ayina, H.L., Roquet, H., 2000. The relationship between the simulated climatic variability modes of the Tropical Atlantic. *Int. J. Climatol.* 20, 939–953.
- Shannon, L., Nelson, G., 1996. The Benguela: large scale features and processes and system variability. In: Wefer, G., Berger, W.H., Sidler, G., Webb, D.J. (Eds.), *The South Atlantic: Present and Past Circulation*. Springer, Berlin, pp. 163–210.
- Shannon, L.J., Field, J.C., Moloney, C.L., 2004. Simulating anchovy–sardine regime shifts in the southern Benguela ecosystem. *Ecol. Model.* 172, 269–281.
- Sherman, K., Belkin, I.M., Friedland, K.D., O'Reilly, J., Hyde, K., 2009. Accelerated warming and emergent trends in fisheries biomass yields of the world's large marine ecosystems. *Ambio Hum. Environ.* 38, 215–224.
- Smith, T.M., Reynolds, R.W., Peterson, T.C., Lawrimore, J., 2008. Improvements to NOAA's historical merged land–ocean surface temperature analysis (1880–2006). *J. Clim.* 21, 2283–2296. <http://dx.doi.org/10.1175/2007JCLI2100.1>.
- Soares, H.C., Pezzi, L.P., Gherardi, D.F.M., Paes, E.D., 2011. Oceanic and atmospheric patterns during spawning periods prior to extreme catches of the Brazilian sardine (*Sardinella brasiliensis*) in the southwest Atlantic. *Sci. Mar.* 75, 665–677. <http://dx.doi.org/10.3989/scimar.2011.75n4665>.
- Thompson, D.W.J., Wallace, J.M., 2000. Annular modes in the extratropical circulation. Part I: month-to-month variability. *J. Clim.* 13, 1000–1016.
- Torrence, C., Compo, G.P., 1998. A practical guide to wavelet analysis. *Bull. Am. Meteorol. Soc.* 79, 61–78.
- Tourre, Y.M., Rajagopalan, B., Kushnir, Y., 1999. Dominant patterns of climate variability in the Atlantic Ocean during the last 136 years. *J. Clim.* 12, 2285–2299.
- Wainer, I., Venegas, S.A., 2002. South Atlantic multidecadal variability in the climate system model. *J. Clim.* 15, 1408–1420.
- Wang, C., 2002. Atlantic climate variability and its associated atmospheric circulation cells. *J. Clim.* 15, 1516–1536.
- Wang, B., An, S.I., 2002. A mechanism for decadal changes of ENSO behavior: roles of background wind changes. *Clim. Dyn.* 18, 475–486.
- Wang, M., Overland, J.E., Bond, N.A., 2010. Climate projections for selected large marine ecosystems. *J. Mar. Syst.* 79, 258–266.
- Wu, L., Zhang, Q., Liu, Z., 2004. Towards understanding tropical Atlantic variability using coupled modeling surgery. In: Wang, C., Xie, S.-P., Carton, J.A. (Eds.), *Earth's Climate: The Ocean–Atmosphere Interaction*. AGU, Washington DC, pp. 157–170.
- Wu, L., He, F., Liu, Z., Li, C., 2007. Atmospheric teleconnections of Tropical Atlantic variability: interhemispheric, tropical–extratropical, and cross-basin interactions. *J. Clim.* 20, 856–870.
- Xie, S.-P., 1999. A dynamic ocean–atmosphere model of the Tropical Atlantic decadal variability. *J. Clim.* 12, 64–70.
- Zebiak, S.E., 1993. Air–sea interaction in the tropical Atlantic region. *J. Clim.* 6, 1567–1586.
- Zhang, Y., Wallace, J.M., Battisti, D.S., 1997. ENSO-like interdecadal variability: 1900–93. *J. Clim.* 10, 1004–1020.